

Article

A Novel Comparative Statistical and Experimental Modeling of Pressure Field in Free Jumps along the Apron of USBR Type I and II Dissipation Basins

Seyed Nasrollah Mousavi ¹  and Daniele Bocchiola ^{2,*} ¹ Department of Water Engineering, University of Tabriz, Tabriz 5166616471, Iran; s.n.mousavi@tabrizu.ac.ir² Department of Civil and Environmental Engineering, Politecnico di Milano, L. da Vinci, 32, 20133 Milano, Italy

* Correspondence: daniele.bocchiola@polimi.it

Received: 7 September 2020; Accepted: 29 November 2020; Published: 3 December 2020



Abstract: Dissipation basins are usually constructed downstream of spillways to dissipate energy, causing large pressure fluctuations underneath hydraulic jumps. Little systematic experimental investigation seems available for the pressure parameters on the bed of the US Department of the Interior, Bureau of Reclamation (USBR) Type II dissipation basins in the literature. We present the results of laboratory-scale experiments, focusing on the statistical modeling of the pressure field at the centerline of the apron along the USBR Type I and II basins. The accuracy of the pressure transducers was $\pm 0.5\%$. The presence of accessories within basin_{II} reduced the maximum pressure fluctuations by about 45% compared to basin_I. Accordingly, in some points, the bottom of basin_{II} did not collide directly with the jet due to the hydraulic jump. As a result, the values of pressure and pressure fluctuations decreased mainly therein. New original best-fit relationships were proposed for the mean pressure, the statistical coefficient of the probability distribution, and the standard deviation of pressure fluctuations to estimate the pressures with different probabilities of occurrence in basin_I and basin_{II}. The results could be useful for a more accurate, safe design of the slab thickness, and reduce the operation and maintenance costs of dissipation basins.

Keywords: basin_I; basin_{II}; mean pressure head; pressure head with different probabilities of occurrence; standard deviation of the pressure fluctuations; statistical modeling; USBR

1. Introduction

Hydraulic jump with the turbulent entrainment process is a function of time and position. This phenomenon is a complex and stochastic process, so that hydrodynamic pressure fluctuations can be analyzed using statistical methods. Energy dissipation through the hydraulic jumps with the conversion of energy downstream of spillways is usually confined within the dissipation basins [1]. This type of hydraulic structure protects the soil against flow erosion, which can affect the dam's safety. Due to the large heads upstream of spillways, dissipation basins may be subjected to enormous instantaneous pressure and velocity fluctuations, causing significant stresses in such energy dissipators. This may cause the uplift of a basin lining, making it necessary to provide this structure with sufficient weight or anchorage. Through the analysis of collected data, it is possible to characterize the forces under a hydraulic jump according to the values of mean pressures, pressure fluctuations, and extreme pressures [2].

US Department of the Interior, Bureau of Reclamation (USBR) Type II dissipation basins [3] are designed to reduce excess kinetic energy downstream of the spillway [4–10], reduce largely ($\approx 30\%$) the required length compared to smooth basins [11], and help in reducing the costs of the structure [12].

Furthermore, knowledge of the geometric characteristics of the hydraulic jump is fundamental for the design of the dissipation structures. Measurement of fluctuating pressures or forces may be difficult to carry out in the field or at the scale of real structures. Overall, there is a lack of information concerning the hydrodynamic loading on the bottom slabs. Little systematic experimental investigation seems available for Type II dissipation basins, and only a general understanding of the hydraulic behavior is attained [13]. A better understanding of the distribution of pressure fluctuations may lead to a more economical design with high safety of energy dissipation structures.

Toso and Bowers [14] stated that the peak value of the pressure fluctuations intensity coefficient (C'_p) varies up to 60% when comparing results from different works. It seems that these differences were related to the degree of development (larger or smaller) of the flow boundary layer. Accordingly, the fully developed flows show lower values of C'_p than undeveloped ones. Endres [15] developed a real-time acquisition system and treatment of data representative of the instantaneous pressure fields in a hydraulic jump by analyzing instantaneous pressures downstream of a spillway. Pinheiro [16] measured the pressure fields inside the hydraulic jump downstream of a spillway. He concluded that the pressure fields near the bottom and along the hydraulic jump are lower than the corresponding depth of the mean flow. Marques et al. [17] measured pressures within a dissipation basin with the smooth bed downstream of a spillway. They proposed a dimensionless methodology that groups the fluctuating pressures with different incident Froude numbers (Fr_1) in a single trend, being a function of the jump position. The values of Fr_1 used by Endres [15], Pinheiro [16], and Marquez et al. [17] were in the range of 4.2 to 8.6, 6 to 10, and 5 to 8, respectively. Based on the pressure data by Enders [15], Teixeira [18] proposed second-order polynomial relationships for estimating different pressure parameters in smooth dissipation basins.

According to Alves [2], the measurement of fluctuating pressures is highly influenced by laboratory conditions. This may include the Reynolds number of flow, transducer accuracy, transducer installation method, hose length, pressure point diameter, channel width, model roughness, etc. Farhoudi et al. [19] studied the pressure fluctuations around some chute blocks in a St. Anthony Fall (SAF) type dissipation basin. Novakoski et al. [20] showed that the negative pressures in the zone near the spillway toe represent the risk of cavitation in the dissipation basin. They concluded that the extreme pressures with the probabilities of occurrence equal to 0.1% and 1% require careful assessment. Macián-Pérez et al. [21] used a numerical model to analyze pressure distributions in a USBR Type II dissipation basin. Hampe et al. [22] estimated extreme pressures in hydraulic jumps with low Froude numbers. Samadi et al. [23] used some explicit data-driven approaches to estimate the C'_p coefficient underneath hydraulic jumps on a sloping channel.

Mousavi et al. [24] focused on the minimal and maximal pressures, the pressure coefficients, the power spectral density (PSD), the probability density function (PDF), and the uncertainty analysis of the pressures along a USBR Type I basin ($basin_I$). Mousavi et al. [25] assessed the statistical parameters of free jumps, including mean pressure (P^*_m), the standard deviation of pressure fluctuations (σ^*_X), the probability distribution coefficient ($N_{K\%}$), and the pressures with different probabilities ($P^*_{K\%}$) along $basin_I$. Mousavi et al. [26] evaluated artificial intelligence models to estimate the C'_p coefficient for the free and submerged jumps at the bottom of a USBR Type II basin ($basin_{II}$). The results showed the deep learning model could estimate the C'_p coefficient more accurately.

However, pressure patterns on the apron of $basin_{II}$ have not been widely investigated in the literature. We designed and pursued experiments to obtain some information about the effect of chute blocks and dentated end sill on the free jumps' characteristics and pressure fluctuation. Experiments were conducted in the centerline of the apron along $basin_I$ and $basin_{II}$ with the incident Froude numbers (Fr_1) in the range of 6.14 to 8.29. In summary, the differences between the previous works and the present paper are explained as follows:

- i. Analysis of the minimal and maximal values of pressures along the free jumps within $basin_I$ and $basin_{II}$. These parameters for $basin_{II}$ have not been investigated in the literature.

- ii. Evaluation of the PSD analysis to determine the dominant frequency of fluctuating pressures in the free jumps for basin_I and basin_{II}. In addition, assessment of the PDF histograms for the fluctuating pressures at different pressure points and investigation of the skewness and kurtosis coefficients, P_m^* , extreme pressures (P_{min}^* and P_{max}^*), σ_X^* , $N_{K\%}$, and $P_{K\%}^*$ along basin_I and basin_{II}. For reference, we benchmarked and compared our findings with previous similar results of other authors focusing on hydraulic jumps we could retrieve in the present literature.
- iii. Proposition of some new original best-fit relationships to estimate the dimensionless forms of statistical parameters including P_m^* , σ_X^* , $N_{K\%}$, and $P_{K\%}^*$ for the free jumps as a function of the dimensionless position along basin_I and basin_{II}.
- iv. Proposition of the hydraulic jump length (L_j) as a scaling factor for the dimensionless position from the toe of the spillway (X^*). Marques al. [17] proposed the dimensionless adjustments for the pressure parameters. Due to the presence of significant air bubbles at the beginning of the jump, it is difficult to measure the initial depth of the jump (Y_1) with great accuracy. It seems that the expression of $Y_2 - Y_1$ (conjugated depths of hydraulic jumps) is not appropriate as a scaling factor. In this case, the X^* parameter was defined as X/L_j , where L_j is the length of hydraulic jump. In addition, the values of Y_1 were calculated using the well-known equation of Bélanger [27].

2. Materials and Methods

2.1. Experimental Setup

In this research, the pressure field of free jumps was investigated in the hydraulic laboratory, University of Tabriz, Iran (see Figure 1). The laboratory flume used had a length of 10 m, a width of 0.51 m, and a height of 0.5 m. The channel's bed was considered in the form of a horizontal line in all experiments. An Ogee spillway of 70 cm in height (H) was equipped with two different configurations of the dissipation basins, designed according to the USBR criteria [3]. In addition, the accessories of basin_{II}, including eight chute blocks (3.2 cm width, 3 cm height, and 7.94 cm length) and a dentated end sill with 6 cm height, were designed based on the maximum flow discharge. The spillway was installed at a distance of 260 cm from the entrance head tank of the flume.

We performed some experiments on basin_I and basin_{II} with different flow discharges, ranging from 33 to 60.4 L/s, and supercritical Froude numbers (Fr_1) between 6.14 and 8.29. According to the USBR recommendation, the lengths of basin_I (L_I) and basin_{II} (L_{II}) were 200 and 125 cm, respectively. The width of the basins was considered equal to the width of the flume (see Figure 2). At the end of the flume, a hinged weir was used to create and stabilize the free jump position. Therefore, the hydraulic jump was positioned at the basins' beginning and contained within the basins (i.e., jump type A-jump [28]).

The subcritical flow depth (Y_2) at the endpoint of the jumps was measured along the flume's centerline. To do this, we used a Data logic ultrasonic sensor device model US30, made in Italy with a nominal accuracy of 1 mm. The discharge in the flume (Q) was measured with a transit-time clamp-on ultrasonic flow meter. The values of supercritical flow depth (Y_1) were calculated using the Bélanger's equation [27,29,30], which is defined as follows:

$$\frac{Y_1}{Y_2} = \frac{1}{2}(-1 + \sqrt{1 + 8 Fr_2^2}) \quad (1)$$

$$Fr_2 = \frac{V_2}{\sqrt{g \times Y_2}} \quad (2)$$

where V_2 is the mean subcritical velocity, calculated using the continuity law, Fr_2 is the subcritical Froude number, and g is the gravitational acceleration.

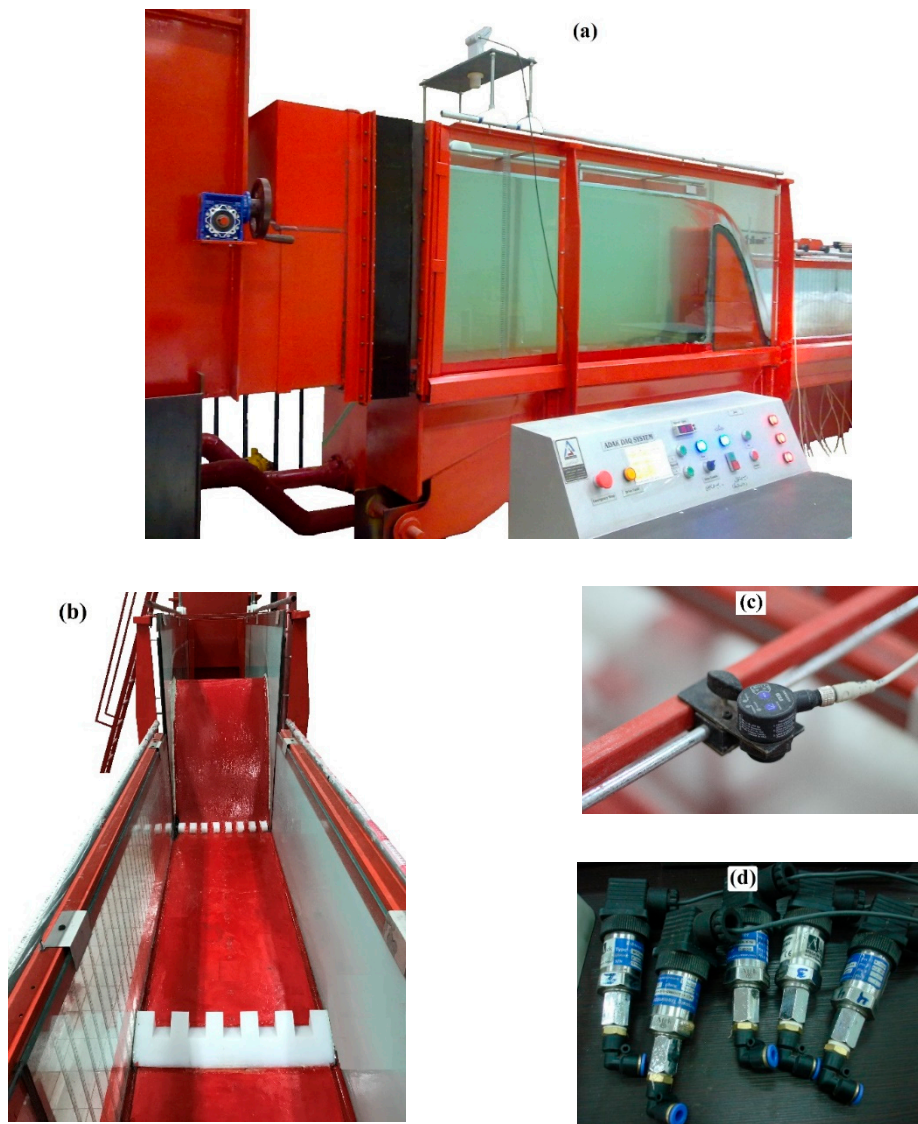


Figure 1. Laboratory flume and experimental setup. (a) Hydraulic jump during an experiment, (b) basin_{II} with chute blocks and dentated end sill, (c) Data logic ultrasonic sensor device model US30, and (d) pressure transducers (Atek BCT 110 series with 100 mbar-A-G1/4 model).

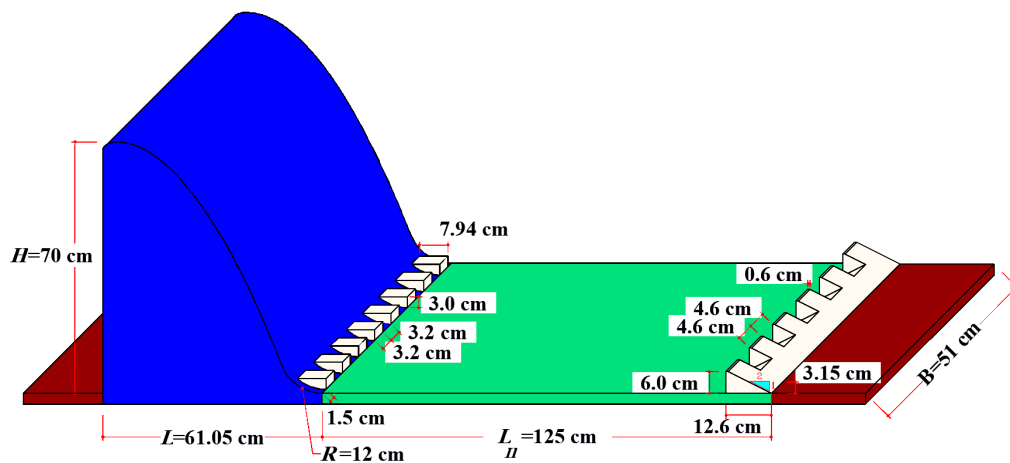


Figure 2. Dimensions of spillway and accessories installed in basin_{II}.

To measure the (dynamic) pressure fluctuations, 25 measurement points were considered along the centerline of the apron inside and outside the basin_{II} (see Figure 3). Pressure therein was measured by way of piezometers installed at the centerline of the apron along the basins. The position of the pressure points (X) was from 2.5 cm (piezometer No. 1) to 189 cm (piezometer No. 25). The instantaneous pressures were measured with pressure transducers (Atek BCT 110 series with 100 mbar-A-G1/4 model). The pressure transducers used a 6-channel digital board and have an accuracy of $\pm 0.5\%$ within the range of -1.0 to 1.0 m [24–26].

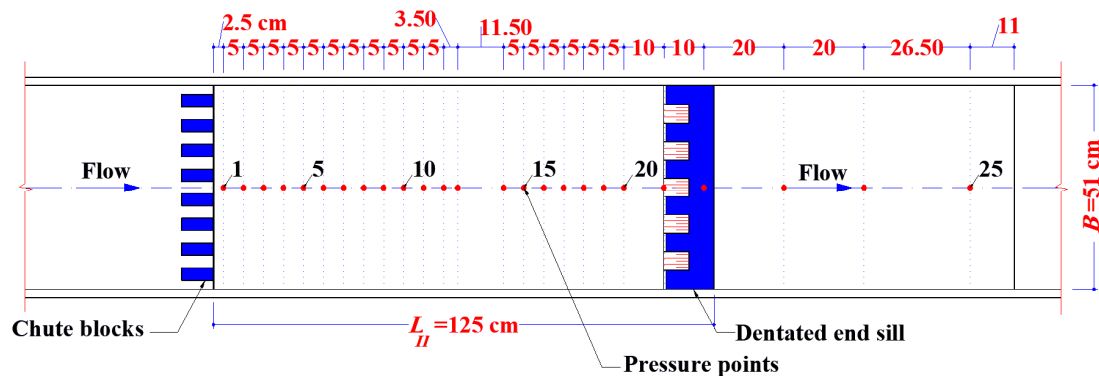


Figure 3. Distribution of the pressure points at the centerline of the apron along basin_{II}.

Pressure transducers were calibrated before the experiments using a static pressure gauge in the laboratory. Therefore, the mean fluctuating pressures were approximately equal to the static pressures. The transducers were mounted on a support plate, placed under the bottom of the flume. Thus, it was possible to eliminate possible distortion effects in the pressure signal due to the connection with rubber hoses. The transparent plastic hoses used here had an internal diameter of 3 mm and were 200 cm in length. Hydrodynamic pressure data were measured in time series. Accordingly, some statistical methods were used to analyze the collected pressure data.

2.2. Statistical Parameters

Investigation of the pressure head (cm) parameter is a first step to describe the pressure field in the hydraulic jump. The pressure parameters at each point (P_X) include the minimum pressure (P_{min}), the mean pressure (P_m), the maximum pressure (P_{max}), and the pressure with a certain probability of occurrence ($P_{K\%}$). Marques et al. [17] proposed $P^*_X = (P_X - Y_1)/(Y_2 - Y_1)$ for the dimensionless form of pressure parameters as a function of the dimensionless position of each point (X^*), defined as $X^* = X/(Y_2 - Y_1)$, where X is the longitudinal position of each point inside the hydraulic jump. As the upstream part of the jump exhibited significant air bubbles, it seems that the scaling of $Y_2 - Y_1$ is not appropriate for the non-dimensional position of the pressure point. As a result, in the present study, the X^* parameter was defined as X/L_j , where L_j is the hydraulic jump length.

Knowledge of the extreme pressure heads in the dissipation basins helps to understand the energy dissipation of the hydraulic jumps. In the present study, the extreme pressure heads (P^*_{min} and P^*_{max}) were investigated in detail. Marques et al. [17] proposed $(\sigma^*_X/E_l) \times (Y_2/Y_1)$ to analyze the dimensionless standard deviation of the pressure fluctuations at point X . There, E_l is energy head loss (cm) along the hydraulic jump. The experimental values of $P_{K\%}$ were achieved using the pressure time series data collected at each pressure point. The statistical coefficient of the probability distribution ($N_{K\%}$) can be varied at different points of the dissipation basins. Therefore, it is necessary to determine the longitudinal distribution of $N_{K\%}$ to estimate the $P^*_{K\%}$ parameter with a probability to be less than or equal to a certain value (K) along basin_I and basin_{II}. As the estimated values of P_m , σ_X , and $N_{K\%}$ were determined at each point inside the basins, the values of $P_{K\%}$ can be estimated using equation $P_{K\%} = P_m + N_{K\%} \times \sigma^*_X$ [17].

In this study, a new statistical methodology was proposed to estimate the values of $P^*_{K\%}$ in basin_I and basin_{II}. To evaluate the estimated values of pressure parameters, some statistical performance criteria were determined [31–34]. The PDF function of the normalized pressures along the hydraulic jumps was calculated according to $P^*(Z) = (1/\sqrt{2\pi}) \times \text{Exp}(-Z^2/2)$. The normalized pressure variable (Z) was defined as $(P[X,t] - P_m)/\sigma_X$, where $P[X,t]$ is the instantaneous pressure [35]. We pursued an analysis of the skewness and kurtosis coefficients of pressure fluctuations [36]. Due to the high variation in S and K coefficients, it is difficult to define a single statistical distribution to describe the overall behavior along the jump.

3. Results and Discussion

3.1. Flow Characteristics

Table 1 presents some experimental and calculated parameters of the flow downstream of the spillway in two dissipation basins under different free jump conditions.

Table 1. Experimental parameters in two dissipation basins.

Q (L/s)	V ₁ (m/s)	Fr ₁	Re ₁	Y ₁ (cm)	Y ₂ (cm)		L _j (cm)	
					basin _I	basin _{II}	basin _I	basin _{II}
33.0	3.52	8.29	58,200	1.84	20.65	19.69	142.50	102.50
43.0	3.59	7.48	74,400	2.35	23.70	22.44	162.50	112.50
47.5	3.60	7.14	81,500	2.59	24.87	23.57	189.00	122.50
52.7	3.58	6.72	89,500	2.89	26.05	24.70	189.00	122.50
55.0	3.56	6.52	92,900	3.03	26.49	25.33	189.00	122.50
60.4	3.53	6.14	100,900	3.36	27.55	26.60	189.00	122.50

₁ Supercritical flow, ₂ Subcritical flow.

Re₁ is the Reynolds number for the supercritical flow of the hydraulic jump. The mean velocity of the incoming flow to the dissipation basins (V_1) was computed using the continuity law. According to Table 1, the Y_2 parameter in basin_{II} decreases compared to those in the basin_I case (classical hydraulic jump). As Q increases, Y_1 increases faster than V_1 . Accordingly, the Froude number reduces when increasing flow discharges. The flow conditions downstream of the spillways are different compared to the sluice gates. The Y_1 parameter has an essential role in determining the values of Fr_1 . Reducing Fr_1 with increasing Q for the free jumps downstream of the spillway has been confirmed in previous similar results we were able to retrieve in the present literature [13,17,37,38].

3.2. Power Spectral Density Analysis

The power spectral density (PSD) analysis of the pressure data demonstrates the variation of the PSD parameter in a wide range of frequencies. According to Figure 4, the maximum values of the amplitude corresponding to the dominant frequency decrease by increasing distance from the jump toe. The results indicated that the maximum variation of the PSD parameter in free jumps within basin_{II} was achieved at frequencies less than 5 Hz. It should be noted that the PSD analysis of the fluctuating pressures for different points of basin_I with free jumps has been studied by Mousavi et al. [24]. The minimum frequency of pressure transducers is considered to be almost twice the dominant frequency of the signal in the literature [39]. In the present study, a pressure data collection frequency of 20 Hz for 90 s was used for each pressure point. The maximum amplitude at low frequencies along the free jumps indicates large-scale vortices, which is due to the dominance of gravitational forces [40]. Therefore, the Froude law is valid for modeling fluctuating pressures in free jumps.

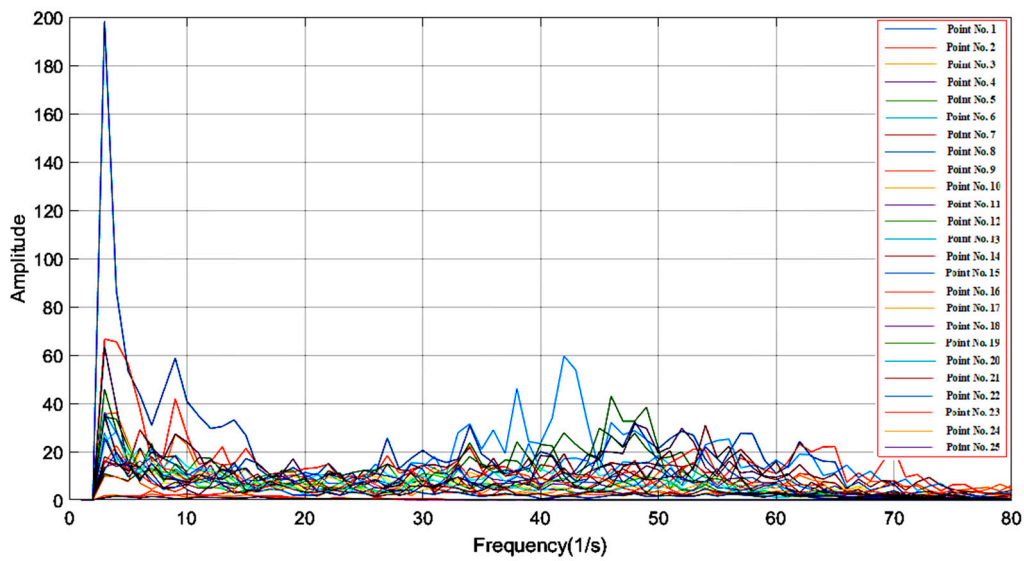


Figure 4. Power spectral density (PSD) analysis of fluctuating pressures for basin_{II} ($Fr_1 = 6.14$).

3.3. Probability Density Function

In this section, the $P^*(Z)$ parameter is plotted as a function of the normalized pressure level (Z). Furthermore, the appropriate probability distributions for each pressure point are compared with the normal distribution. The PDF histograms of pressure fluctuations at some points on the bed of basin_{II} in free jumps are shown in Figure 5. In addition, the PDF function of the fluctuating pressures for different points of basin_I with the free jumps has been previously investigated by Mousavi et al. [24]. The results indicate that the PDF function does not follow the normal distribution at different points along the free jumps, especially for the initial points of basin_{II}. In other words, the S and K coefficients do not match with the normal distribution values.

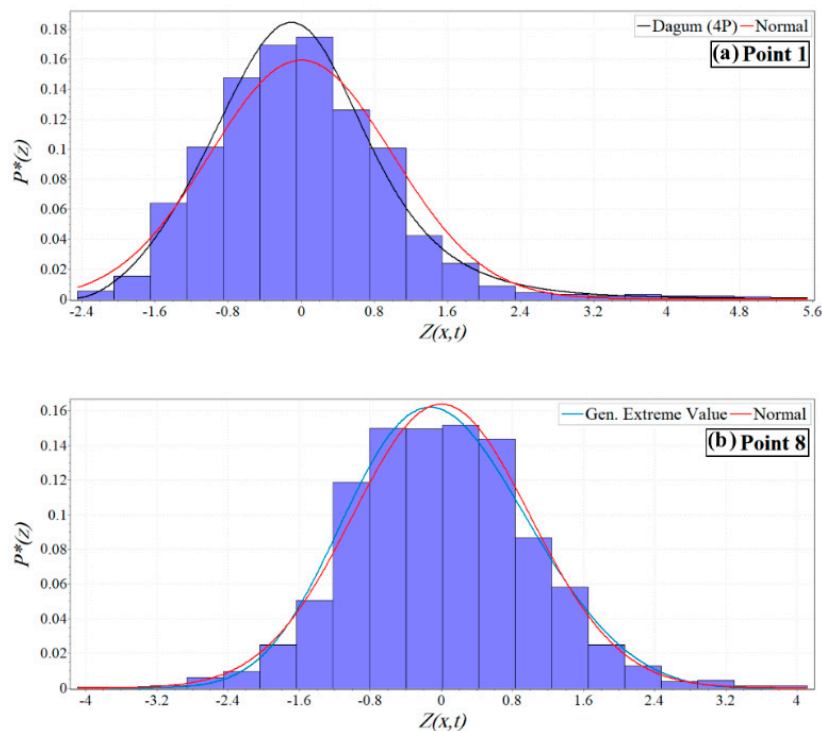


Figure 5. Cont.

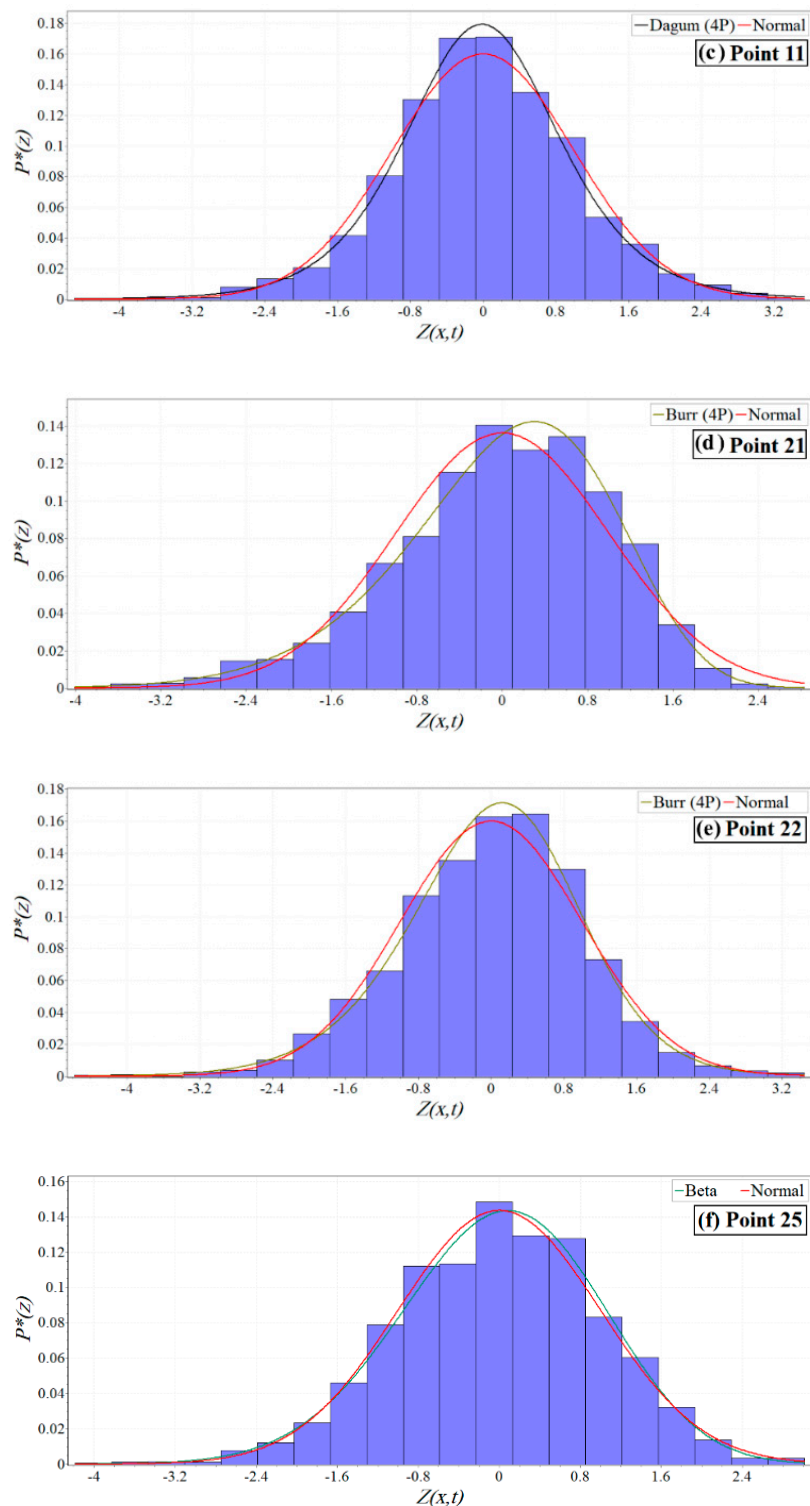


Figure 5. Probability density function (PDF) histograms of fluctuating pressures at some points of basin_{II} ($Fr_1 = 6.14$): (a) point 1; (b) point 8; (c) point 11; (d) point 21; (e) point 22; (f) point 25.

According to Fiorotto and Rinaldo [35], positive pressure fluctuations at the beginning of the basins have a relatively high frequency compared to negative pressure fluctuations. In this zone, the S coefficient has positive and maximum values, and the PDF curve tail is drawn to the right. The K values are more than the normal distribution, and the PDF curve is drawn upwards at these points.

At the characteristic point of X^*_d (point of expected flow detachment), the frequency of positive and negative pressure fluctuations is almost identical, and $S \approx 0$ (pressure point No. 11). At this point, pressure values distribution is somewhat similar to the normal distribution. For point No. 21, located at X^*_r (endpoint of the roller), the S coefficient has negative values. Also, the K coefficient is greater than the normal distribution value. For points located at X^*_j (endpoint of the hydraulic jump), the S values tend to move towards zero, and the data somewhat follow the normal distribution. Pressure point No. 25 is outside basin_{II}, and it has a normal distribution. The flow energy of the incoming jet is dissipated after passing through the roller point of the jump, and the uniform flow is established almost downstream of the basin. Due to the presence of accessories in basin_{II}, all the considered characteristic points are closer than in the absence of such structures.

3.4. Extreme Pressures

Figure 6 represents variations of the dimensionless minimum, mean, and maximum (scaled) pressures (P^*_{min} , P^*_m , and P^*_{max}) as a function of X^* in basin_{II} and basin_I for different values of Fr_1 . It is observed that the P^*_{min} data reach lower values and have more significant fluctuations concerning the P^*_m data at the position nearest to the spillway toe (probably due to the incidence of flow in the basin).

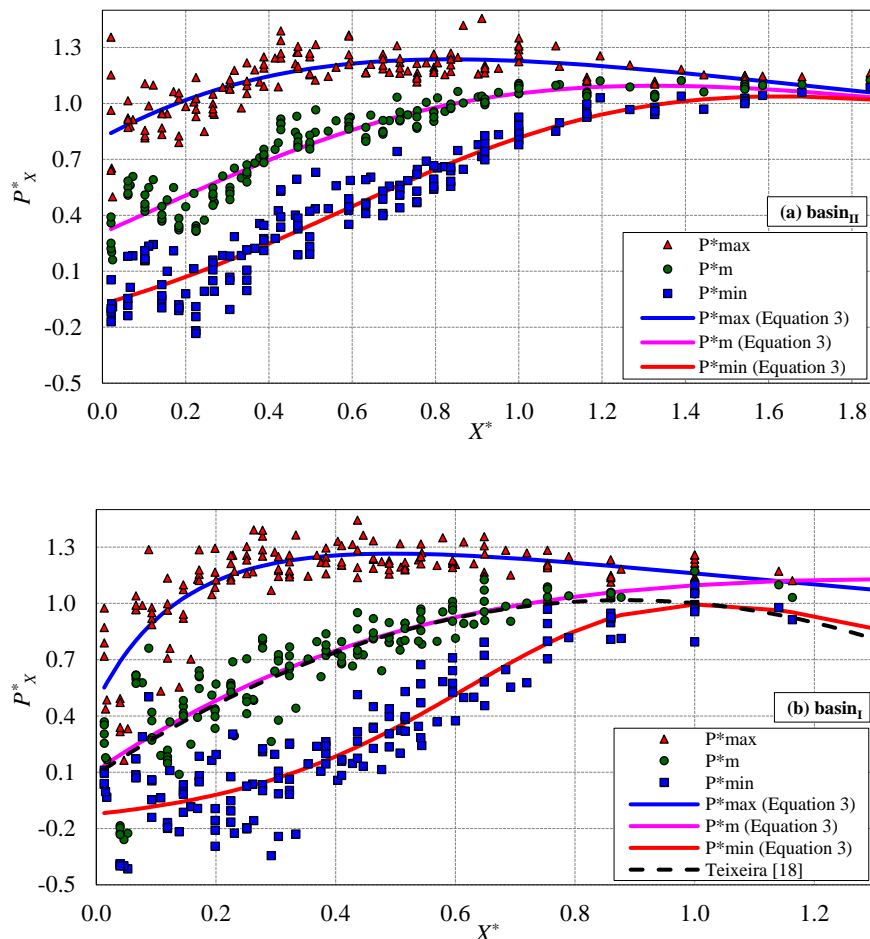


Figure 6. Distribution of the experimental and estimated values of P^*_X : (a) basin_{II}; (b) basin_I.

The P^*_{min} data reach negative values around -0.2 approximately at $X^* \leq 0.20$ for basin_{II}, and of -0.4 at $X^* \leq 0.30$ for basin_I, increasing with oscillations after that. This may indicate zones subject to low pressure, which may be associated with erosion or cavitation processes. Therefore, basin_{II} is more reliable than basin_I in terms of the possibility of cavitation. At the position of X^*_j , P^*_{min} data begin to oscillate near the value 1.0 and slightly lower. Concerning the values of P^*_{max} , the higher and

more disparate values versus the P_m^* values occur near the spillway, caused by the direct impact of the flow jet on the dissipation basins. The values of extreme pressures in basin_{II} are lower than those for basin_I. There is a narrower pressure range in basin_{II} compared to basin_I. The results indicate that P_{max}^* seemingly decreases with the increasing Froude number, with P_m^* and P_{min}^* somewhat constant, in the explored range. Using the results obtained in the present study by adjusting the values of P_X^* , including P_{min}^* , P_m^* , and P_{max}^* , a new second-order rational expression was developed for basin_{II} and basin_I. Equation (3) is valid for $0 < X^* \leq 1.85$ in basin_{II} and $0 < X^* \leq 1.30$ in basin_I. According to Figure 6, one can estimate P_X^* using Equation (3). The values of α , β , γ , and δ to estimate P_X^* for basin_{II} and basin_I are provided in Table 2.

$$P_X^* = \frac{\alpha + \beta X^*}{1 + \gamma X^* + \delta X^{*2}} \tag{3}$$

Table 2. Coefficients of α , β , γ , δ , and the statistical performance criteria to estimate P_X^* .

Basin	P_X^*	A	B	γ	δ	R	RMSE	MAE
basin _{II}	P_{min}^*	-0.0758	0.6885	-0.6537	0.4041	0.950	0.110	0.082
	P_m^*	0.3057	0.9186	-0.2466	0.4086	0.944	0.085	0.063
	P_{max}^*	0.8171	1.5498	0.4397	0.4879	0.753	0.100	0.072
basin _I	P_{min}^*	-0.1220	0.5397	-1.6625	1.0825	0.909	0.155	0.122
	P_m^*	0.1094	2.2112	0.6233	0.4925	0.882	0.150	0.105
	P_{max}^*	0.4690	8.5806	4.2451	2.5554	0.789	0.145	0.099

* Dimensionless value.

3.5. Standard Deviation of Fluctuating Pressures

The σ_X^* parameter is a function of the flow discharge and the pressure point position relative to the beginning of the jump. In Figure 7, increasing flow discharge (i.e., decreasing Froude number) results in σ_X^* increasing. As Q increases, the dynamic energy increases, and the fluctuating component of pressure (P') increases as well, indicating the turbulence intensity of the flow. Along the jump, σ_X^* increases to a maximum value, in the range of $X^* \leq 0.33$ for basin_I and basin_{II}, and decreases after that. It seems that the main factors for the fluctuations of pressures along the jump are turbulent flow, eddies formation, and their movement during the jump. Therefore, in some positions, the interaction of eddies and the basin bed causes a sudden increase in the bed pressure.

Figure 7b shows a comparison of the σ_X^* values in the case of basin_I with the results obtained by Pinheiro [16] and Marques et al. [17] for free jumps. It is seen that our study displays similar patterns to their work. However, in the downstream zone of the basin, σ_X^* values are relatively higher than the results obtained by others. This is likely to be linked to the determination of Y_1 and Y_2 and identification of the initial position of the hydraulic jump. The σ_X^* values for the smooth bed (basin_I) are greater than in basin_{II} with blocks. Accordingly, the presence of accessories within the hydraulic jumps significantly decreases σ_X^* . Figure 7 demonstrates the values of σ_{Xmax}^* for different Froude numbers in basin_{II} and basin_I. A high value of σ_{Xmax}^* may indicate a considerable variation of the dynamic pressures on the bottom slab, damaging the structure. According to Figure 7, as the Froude number (Fr_1) increases, the intensity of pressure fluctuations decreases. According to Teixeira [18], the average value of σ_{Xmax}^* in a smooth basin was about 0.7.

As seen in Table 3, one has $\sigma_{Xmax}^* \approx 0.50\sim 0.68$ for basin_{II}, and $\sigma_{Xmax}^* \approx 1.02\sim 1.20$ for basin_I, similarly for all Froude numbers. Accordingly, the values of σ_{Xmax}^* in basin_{II} decreased down to about -45% compared with basin_I for the free jumps. The $X_{\sigma max}^*$ position in the presence of the blocks and end sill is closer to the spillway toe. The accessories on the bed of basin_{II} may cause the jet to be spread or submerged. Due to the presence of chute blocks at some points, the bottom of basin_{II} does not collide directly with the jet due to the hydraulic jump. Consequently, the values of pressure and

pressure fluctuations decrease mainly therein. Figure 7 illustrates the σ^*_X values for different Froude numbers in basin_{II} and basin_I.

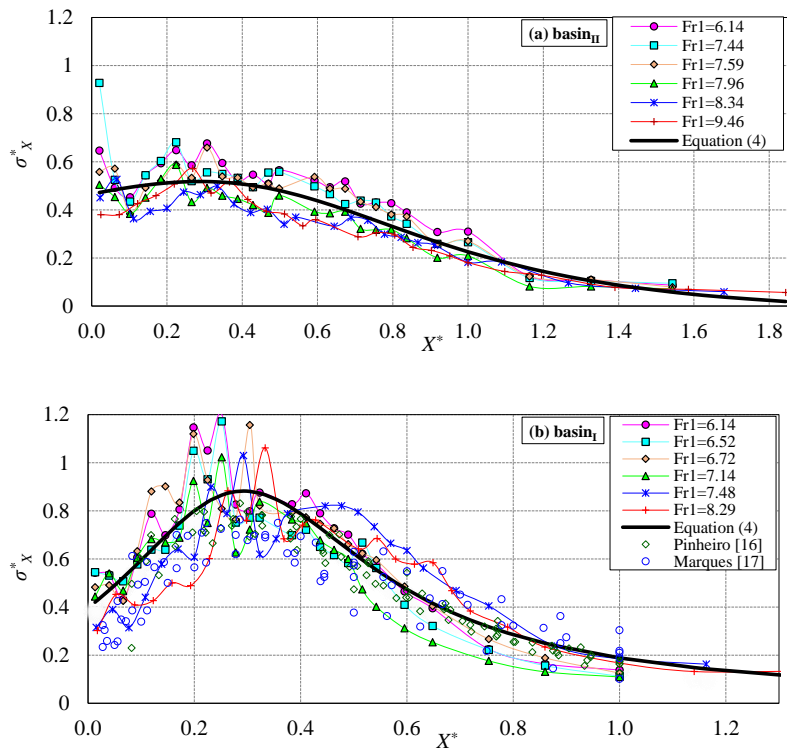


Figure 7. Distribution of the experimental and estimated values of σ^*_X : (a) basin_{II}; (b) basin_I.

Table 3. Range of σ^*_{Xmax} values and the position of $X^*_{\sigma max}$.

Results	σ^*_{Xmax}	$X^*_{\sigma max}$
basin _{II}	0.50~0.68	0.07~0.33
basin _I [25]	1.02~1.20	0.25~0.33
Endres [15]	0.65~0.77	0.03~0.18
Pinheiro [16]	0.73~0.83	0.25~0.33
Marques [17]	0.69~0.76	0.22~0.40

* Dimensionless value.

We optimized Teixeira’s method [18] to assess σ^*_X for basin_{II} and basin_I. A new second-order rational expression was developed in the range of $0 < X^* \leq 1.85$ for basin_{II} and $0 < X^* \leq 1.30$ for basin_I. According to Figure 7, one can estimate σ^*_X using Equation (4). The values of $a, b, c,$ and d to determine σ^*_X are provided in Table 4.

$$\sigma^*_X = \frac{a + b X^*}{1 + c X^* + d X^{*2}} \tag{4}$$

Table 4. Coefficients of $a, b, c, d,$ and the statistical performance criteria to estimate σ^*_X .

Results	a	B	c	d	R	RMSE	MAE
basin _{II}	0.4661	-0.2218	-1.1229	1.2068	0.910	0.065	0.053
basin _I	0.3975	0.3735	-3.3347	6.4248	0.872	0.120	0.095

* Dimensionless value.

Therefore, the new adjustment can estimate σ^*_X very well with a correlation coefficient (R) equal to 0.910 and 0.872 for basin_{II} and basin_I, respectively.

3.6. Statistical Coefficient of the Probability Distribution

Figure 8 presents the distribution of the experimental values of the $N_{K\%}$ coefficient obtained from the pressure data along basin_{II} for different probabilities from 0.1% to 99.9% with different flow conditions in free jumps. The distribution of the $N_{K\%}$ coefficient along basin_I with the free jumps has been previously investigated by Mousavi et al. [25].

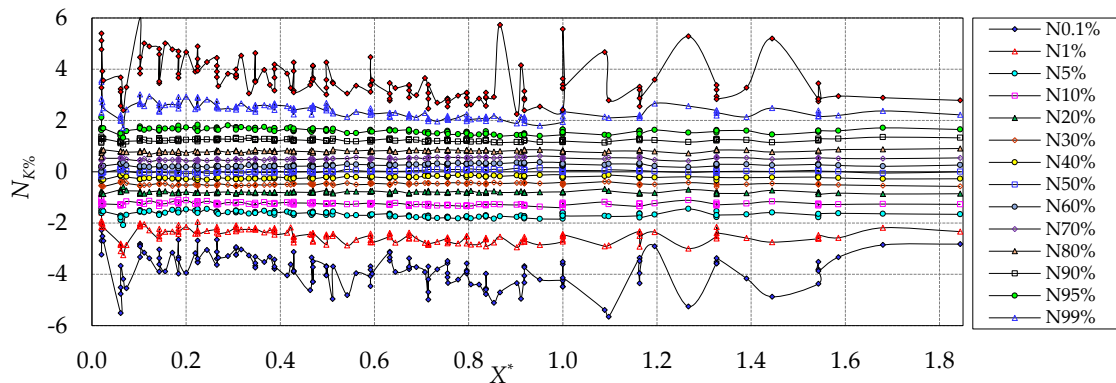


Figure 8. Distribution of the experimental values of the $N_{K\%}$ coefficient along basin_{II}.

From Figure 8, one can verify the dispersion of the $N_{K\%}$ coefficient with the minimum and maximum extreme pressures in the initial zone of the jumps. It is observed that for probabilities greater than 50%, the $N_{K\%}$ coefficient has positive values, and for probabilities less than 50%, it has negative values. At the beginning area of the basins, the values of $N_{0.1\%}$ are approximately -3 , and for positions $X^* \geq 0.40$, it has values less than -4 . In addition, the $N_{99.9\%}$ coefficient at the beginning of basin_{II} has values around 4 to 6. At the downstream of the basins, the $N_{K\%}$ values are slightly stabilized and vary in the range of 2 to 4. The results show that the variation rate of the $N_{K\%}$ coefficient along basin_{II} has decreased somewhat compared to basin_I.

Teixeira [18] demonstrated that in free jumps, the longitudinal distribution of the $N_{K\%}$ coefficient follows a second-order polynomial relationship. In the present study, the results show that the $N_{K\%}$ coefficient has relatively constant values along the jumps, mainly for the probabilities from 5% to 95%. Accordingly, depending on the probability to be identified, the $N_{K\%}$ coefficient shows a trend more or less close to a single (average) value for each probability, regardless of Fr_1 values. Table 5 displays the average experimental values of the $N_{K\%}$ coefficient with different probabilities along the basins.

Table 5. Average experimental values of $N_{K\%}$ coefficient in the dissipation basins.

$N_{K\%}$	$N_{5\%}$	$N_{10\%}$	$N_{20\%}$	$N_{30\%}$	$N_{40\%}$	$N_{50\%}$	$N_{60\%}$	$N_{70\%}$	$N_{80\%}$	$N_{90\%}$	$N_{95\%}$
basin _{II}	-1.66	-1.25	-0.80	-0.48	-0.22	0.02	0.252	0.51	0.80	1.23	1.60
basin _I	-1.62	-1.25	-0.82	-0.50	-0.24	0.00	0.242	0.50	0.81	1.25	1.63

To develop a method for estimating the $P^*_{K\%}$ parameter in the case of basin_{II} and basin_I, we identified variations in the $N_{K\%}$ coefficient as a function of probability. Therefore, it was decided to use the average value of $N_{K\%}$ for each probability. According to Wiest [41], there is little effect of Fr_1 on $N_{K\%}$, and the latter remains constant along the dissipation basin. Accordingly, $N_{K\%}$ follows a specific curve acceptably well, making it possible to establish a new adjustment for $N_{K\%}$ as a function of the probability of occurrence (K). Therefore, we propose a second-order rational relationship to estimate $N_{K\%}$:

$$N_{K\%} = \frac{\alpha + \beta K}{1 + \gamma K + \delta K^2} \tag{5}$$

Here α , β , γ , and δ are the coefficients of Equation (5), and K is the value of the probability in decimal. The values of coefficients in Equation (5) are shown in Table 6. The residual of the

experimental and estimated data set of the $N_{K\%}$ coefficient for different probabilities in basin_{II} and basin_I is plotted in Figure 9. This parameter is defined as the difference between the experimental and estimated values of $N_{K\%}$.

Table 6. Coefficients of Equation (5) for estimating $N_{K\%}$ coefficient in dissipation basins.

Results	α	β	γ	δ
basin _{II}	-2.1625	4.3873	3.8320	-3.7389
basin _I	-2.0752	4.1402	3.3326	-3.3448

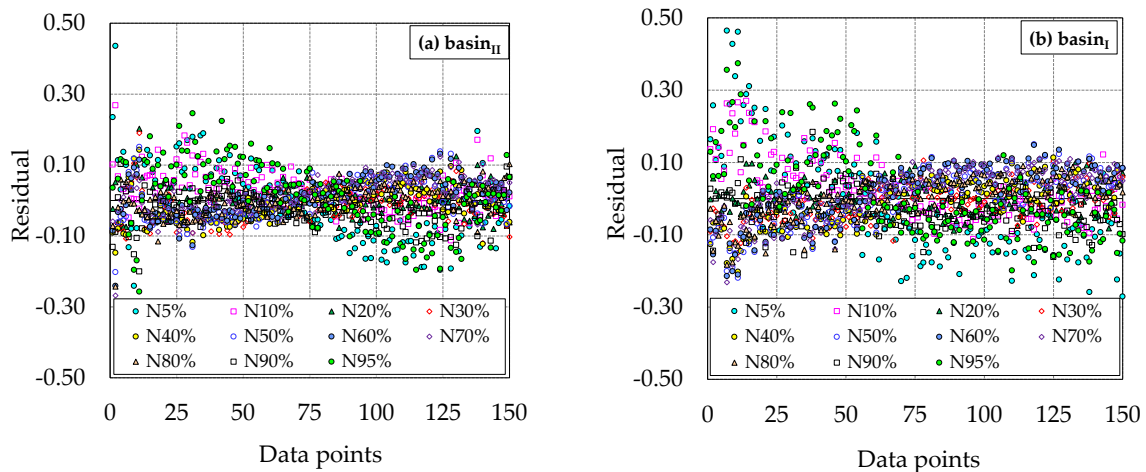


Figure 9. Residual plots of the experimental and estimated data set of the $N_{K\%}$ coefficient for different probabilities: (a) basin_{II} and (b) basin_I.

3.7. Estimation of Pressures with Different Probabilities of Occurrence

In this study, new original adjustments were proposed for P^*_m (Equation (3)), σ^*_X (Equation (4)), and $N_{K\%}$ (Equation (5)) to estimate the pressure values with different probabilities of occurrence ($P_{K\%}$). Therefore, the estimated values of $P_{\alpha\%}$ were determined using Equation $P_{\alpha\%} = P_m + N_{K\%} \times \sigma_X$.

Some statistical criteria for the estimated values of the $P^*_{K\%}$ parameter in basin_{II} and basin_I are presented in Table 7. For instance, the longitudinal distribution of the experimental and estimated data of the $P^*_{K\%}$ parameter with different probabilities along basin_{II} is shown in Figure 10. The distribution of the $P^*_{K\%}$ parameter for different probabilities of occurrence along basin_I with the free jumps has been previously investigated by Mousavi et al. [25].

Table 7. Statistical criteria to estimate $P^*_{K\%}$ with different probabilities of occurrence.

$P^*_{K\%}$	basin _{II}				basin _I			
	R	RMSE	MAE	WI	R	RMSE	MAE	WI
$P^*_{5\%}$	0.948	0.096	0.073	0.973	0.880	0.166	0.122	0.934
$P^*_{10\%}$	0.946	0.094	0.071	0.972	0.879	0.164	0.120	0.933
$P^*_{20\%}$	0.944	0.092	0.069	0.971	0.879	0.161	0.116	0.932
$P^*_{30\%}$	0.944	0.090	0.067	0.970	0.880	0.158	0.112	0.932
$P^*_{40\%}$	0.943	0.088	0.065	0.970	0.882	0.155	0.109	0.933
$P^*_{50\%}$	0.943	0.087	0.063	0.970	0.884	0.152	0.106	0.934
$P^*_{60\%}$	0.940	0.085	0.062	0.969	0.884	0.150	0.103	0.934
$P^*_{70\%}$	0.942	0.082	0.060	0.969	0.884	0.147	0.100	0.934
$P^*_{80\%}$	0.941	0.080	0.059	0.969	0.884	0.145	0.097	0.934
$P^*_{90\%}$	0.939	0.077	0.057	0.968	0.881	0.141	0.093	0.934
$P^*_{95\%}$	0.929	0.078	0.057	0.963	0.848	0.138	0.093	0.933

* Dimensionless value.

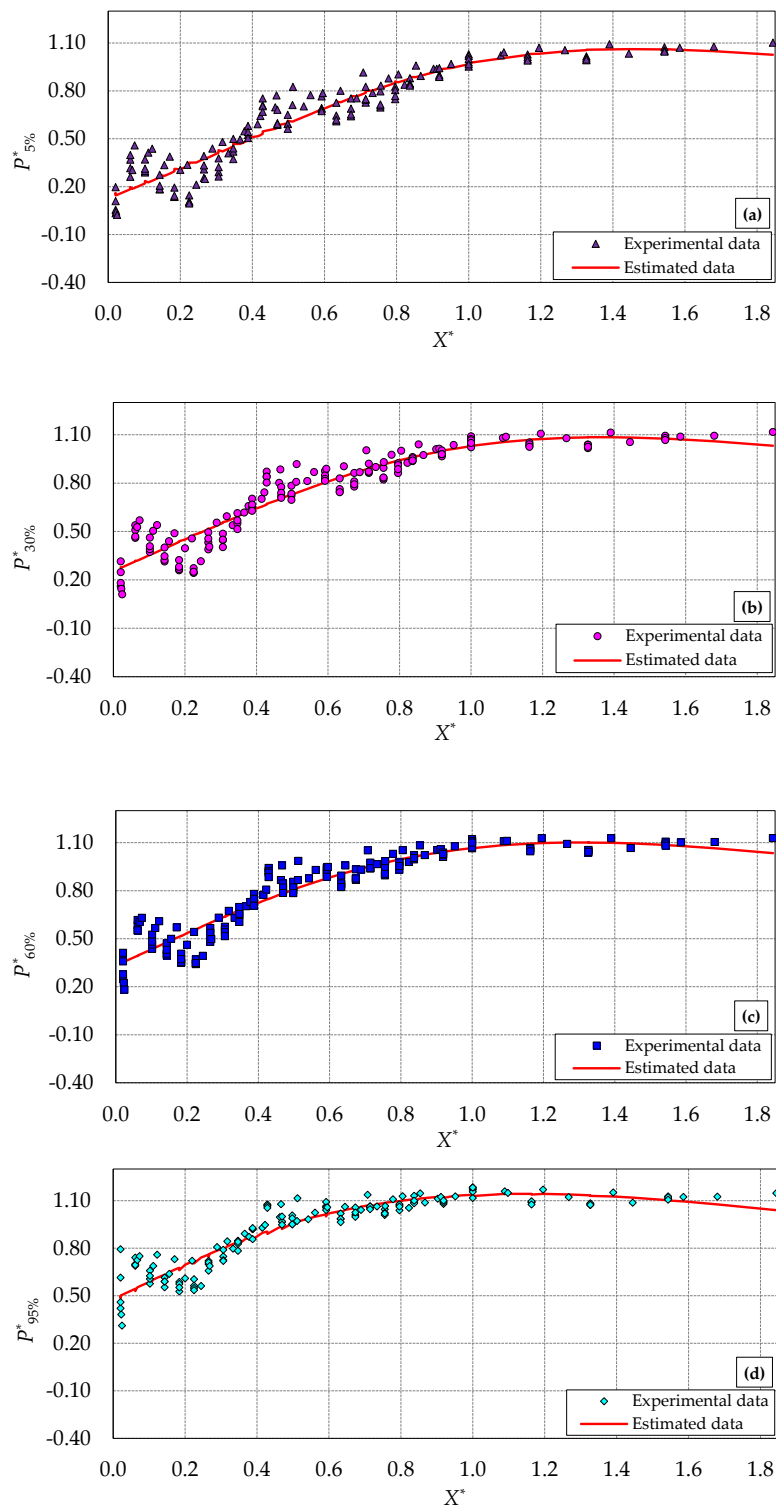


Figure 10. Longitudinal distribution of the experimental and estimated data of $P^*_{K\%}$ parameter with different probabilities along basin II: (a) $P^*_{5\%}$; (b) $P^*_{30\%}$; (c) $P^*_{60\%}$; (d) $P^*_{95\%}$.

4. Conclusions

In this study, a lab-scale model of an Ogee spillway, either equipped with the USBR Type I and II dissipation basins was installed downstream of an Ogee spillway, based on the USBR criteria, to investigate pressure fields therein. The present study aimed to measure and provide useful insights

about the pressure fluctuations at the bottom of basin_{II}. We can provide here some conclusions from our research, covering the (different) patterns of pressures along the free hydraulic jumps, as follows:

- (i) For the first time to our knowledge, our results allow calculation of the statistics and extreme values of the pressure field occurring on the bed of the dissipation basins, and demonstrate the advantage of using a USBR Type II basin in terms of reduced stress over the basin's bed.
- (ii) The Y_2 parameter in basin_{II} was decreased against that in basin_I. In addition, with increasing flow discharge (Q), supercritical flow depth (Y_1) increased more than velocity (V_1). As a result, Fr_1 reduced with higher Q values.
- (iii) The P_{min}^* data reached negative values of around -0.2 approximately at $X^* \leq 0.2$ for basin_{II}, and of -0.4 at $X^* \leq 0.3$ for basin_I (i.e., very close to spillway toe). Therefore, basin_{II} was more reliable than basin_I in terms of the possibility of cavitation. More fluctuating values of P_{max}^* against the mean values occurred near the spillway, justified by the direct impact of the flow jet on the dissipation basin.
- (iv) Analysis of σ_X^* showed that the dimensionless position of $X_{\sigma_{max}}^*$ is close to 0.20 and 0.29 for basin_{II} and basin_I, respectively, with pressure fluctuations decreasing after that. Accordingly, the position of $X_{\sigma_{max}}^*$ was closer to the spillway toe for basin_{II}. With increasing flow discharge, the pressure fluctuations increased. The pressure fluctuations range on the basin bed was visibly narrower for basin_{II} than for basin_I. For basin_{II}, $\sigma_{X_{max}}^*$ values along the free jumps were reduced by -40% compared to basin_I.
- (v) Based on the methodologies proposed by Marques et al. [17] and Teixeira [18], new original best-fit adjustments were proposed here for the P_{m}^* , σ_X^* , and $N_{K\%}$ parameters to estimate the $P_{K\%}^*$ parameter in the case of basin_I and basin_{II}. In addition, we originally displayed that $N_{K\%}$ values show a trend towards a single average value independently of the Froude number, and we proposed an adjustment for $N_{K\%}$ as a function of probability.
- (vi) Some effort may be devoted to investigating the statistical distribution of pressures on the basin bed. As observed, a deviation of the skewness from the $S = 0$ value for normal distribution in the beginning area of the basins indicates a different and asymmetric distribution. Positively skewed distributions indicate the potential for more (than normally expected) frequent outbursts of large flow pressure, possibly requiring the increase of the structural resistance of the basin apron.
- (vii) The laboratory-scale models presented herein have several limitations that should guide further research on the topic. It should be noted that there is a potential error in scaling the pressure heads. Therefore, just indicating the dimensionless terms may be misleading.
- (viii) The results of this work contribute to the present debate about the use of dissipation basins, and especially of USBR Type II ones for spillway flow calming, providing a quantitative assessment of some main features of the hydraulic jump within the dissipation basin, and the modified (reduced) maximum pressure on the basin apron, and are potentially useful for designing dissipation basins in real-world applications.

Author Contributions: Methodology, S.N.M. and D.B.; validation, D.B.; writing—original draft, S.N.M.; writing—review and editing, D.B. Both authors have read and agreed to the published version of the manuscript.

Funding: This research received no external funding.

Acknowledgments: All co-authors would like to express their gratitude to the editors and reviewers for their time spent reviewing our manuscript and for helping to improve the manuscript. Daniele Bocchiola acknowledges the support from the Climate-Lab of the Polytechnic University of Milan (<https://www.climatelab.polimi.it/en/>), an interdepartmental laboratory on climate change at the Polytechnic University of Milan.

Conflicts of Interest: The authors declare no conflict of interest.

Abbreviation

The following symbols are used in this paper:

B	Basin width (L)
$basin_I$	USBR Type I dissipation basin
$basin_{II}$	USBR Type II dissipation basin
C'_p	Pressure fluctuations intensity coefficient
E_l	Energy head loss along the hydraulic jump (L)
Fr_1	Supercritical Froude number
Fr_2	Subcritical Froude number
g	Gravitational acceleration (LT^{-2})
H	Ogee spillway height
K	Kurtosis coefficient
L_I	Length of basin _I (L)
L_{II}	Length of basin _{II} (L)
L_j	Length of hydraulic jump (L)
MAE	Mean absolute error
$N_{K\%}$	Statistical coefficient of the probability distribution
$P_{K\%}$	Pressure head with a certain probability of occurrence (L)
P_{min}	Minimum extreme pressure (L)
P_m	Mean pressure head at each pressure point (L)
P_{max}	Maximum extreme pressure (L)
PSD	Power spectral density of the pressure data
$P(X,t)$	Instantaneous pressure (L)
P^*_Z	Probability density function (PDF) of the normalized fluctuating pressures
P'	Fluctuating component of pressure (L)
Q	Flow discharge (L^3T^{-1})
R	Correlation coefficient
Re_1	Reynolds number for the supercritical flow of the hydraulic jump
RMSE	Root mean squared error
S	Skewness coefficient
USBR	US Department of the Interior, Bureau of Reclamation
V_1	Mean velocity of the coming flow to the dissipation basin (LT^{-1})
V_2	Mean subcritical velocity (LT^{-1})
WI	Willmott's index of agreement
X	Longitudinal position of each point inside the hydraulic jump (L)
X^*	Dimensionless position of each point (X/L_j)
X^*_d	Characteristic point of the expected flow detachment
X^*_r	Characteristic endpoint of the roller
X^*_j	Characteristic endpoint of the hydraulic jump
Y_1	Supercritical flow depth at the jump toe (L)
Y_2	Subcritical flow depth at the end of the jump (L)
Z	Normalized pressure variable
σ_X	Standard deviation of the pressure fluctuations at point X (L)
σ^*_X	Dimensionless standard deviation of the pressure fluctuations at point X (L)
1	Supercritical flow
2	Subcritical flow
m	Mean value
max	Maximum value
min	Minimum value
*	Dimensionless value

References

1. Khatsuria, R.M. *Hydraulics of Spillways and Energy Dissipators*; Marcel Dekker: New York, NY, USA, 2005.
2. Alves, A.A.M. *Characterization of Hydrodynamic Forces in Dissipation Basins under Hydraulic Jumps with Low Froude Number*; Universidade Federal do Rio Grande do Sul: Porto Alegre, Brazil, 2008. (In Portuguese)
3. USBR. Spillways. In *Design of Small Dams*, 3rd ed.; US Department of the Interior, Bureau of Reclamation: Washington, DC, USA, 1987; pp. 339–437.
4. Mohamed Ali, H. Effect of roughened-bed stilling basin on length of rectangular hydraulic jump. *J. Hydraul. Eng.* **1991**, *117*, 83–93. [[CrossRef](#)]
5. Verma, D.; Goel, A. Stilling basins for pipe outlets using wedge-shaped splitter block. *J. Irrig. Drain. Eng.* **2000**, *126*, 179–184. [[CrossRef](#)]
6. Alikhani, A.; Behrozi-Rad, R.; Fathi-Moghadam, M. Hydraulic jump in stilling basin with vertical end sill. *Int. J. Phys. Sci.* **2010**, *5*, 25–29.
7. Tiwari, H.; Goel, A.; Gahlot, V. Experimental Study of effect of end sill on stilling basin performance. *Int. J. Eng. Sci. Technol.* **2011**, *3*, 3134–3140.
8. Cancian Putton, V.; Marson, C.; Fiorotto, V.; Caroni, E. Supercritical flow over a dentated sill. *J. Hydraul. Eng.* **2011**, *137*, 1019–1026. [[CrossRef](#)]
9. Tiwari, H.; Goel, A. Effect of end sill in the performance of stilling basin models. *Am. J. Civil Eng. Archit.* **2014**, *2*, 60–63. [[CrossRef](#)]
10. Fecarotta, O.; Carravetta, A.; Del Giudice, G.; Padulano, R.; Brasca, A.; Pontillo, M. Experimental results on the physical model of an USBR type II stilling basin. In Proceedings of the River Flow 2016, International Conference on Fluvial Hydraulics, St. Louis, MI, USA, 10–14 July 2016.
11. Chanson, H.; Carvalho, R. Hydraulic jumps and stilling basins. In *Energy Dissipation in Hydraulic Structures*; Chanson, H., Ed.; CRC Press: Leiden, The Netherlands, 2015; pp. 65–104.
12. Vischer, D.; Hager, W.H. *Dam Hydraulics*; Wiley: Ürich, Switzerland, 1998; Volume 2.
13. Padulano, R.; Fecarotta, O.; Del Giudice, G.; Carravetta, A. Hydraulic design of a USBR Type II stilling basin. *J. Irrig. Drain. Eng.* **2017**, *143*, 1–9. [[CrossRef](#)]
14. Toso, J.W.; Bowers, C.E. Extreme pressures in hydraulic-jump stilling basins. *J. Hydraul. Eng.* **1988**, *114*, 829–843. [[CrossRef](#)]
15. Endres, L.A.M. *Contribution to the Development of a System for the Acquisition and Processing of Instantaneous Pressures Data in the Laboratory*; Federal University of Rio Grande do Sul: Porto Alegre, Brazil, 1990. (In Portuguese)
16. Pinheiro, A.A.d.N. *Hydrodynamic Actions in Thresholds for Energy Dissipation Basin by Hydraulic Jumps*; Universidade Técnica de Lisboa: Lisbon, Portugal, 1995. (In Portuguese)
17. Marques, M.G.; Drapeau, J.; Verrette, J.-L. Pressure fluctuation coefficient in a hydraulic jump. *Braz. J. Water Resour. (Rbrh)* **1997**, *2*, 45–52. (In Portuguese)
18. Teixeira, E.D. *Scale Effect on Estimating Extreme Pressure Values on the Bed of the Hydraulic Dissipation Basins*; Universidade Federal do Rio Grande do Sul: Porto Alegre, Brazil, 2008. (In Portuguese)
19. Farhoudi, J.; Sadat-Helbar, S.; Aziz, N.I. Pressure fluctuation around chute blocks of SAF stilling basins. *J. Agric. Sci. Technol.* **2010**, *12*, 203–212.
20. Novakoski, C.K.; Hampe, R.F.; Conterato, E.; Marques, M.G.; Teixeira, E.D. Longitudinal distribution of extreme pressures in a hydraulic jump downstream of a stepped spillway. *Braz. J. Water Resour. (Rbrh)* **2017**, *22*. [[CrossRef](#)]
21. Macián-Pérez, J.F.; García-Bartual, R.; Huber, B.; Bayon, A.; Vallés-Morán, F.J. Analysis of the flow in a typified USBR II stilling basin through a numerical and physical modeling approach. *Water* **2020**, *12*, 227. [[CrossRef](#)]
22. Hampe, R.F.; Steinke Júnior, R.; Prá, M.D.; Marques, M.G.; Teixeira, E.D. Extreme pressure forecasting methodology for the hydraulic jump downstream of a low head spillway. *Braz. J. Water Resour. (Rbrh)* **2020**, *25*, 1–10. [[CrossRef](#)]
23. Samadi, M.; Sarkardeh, H.; Jabbari, E. Explicit data-driven models for prediction of pressure fluctuations occur during turbulent flows on sloping channels. *Stoch. Environ. Res. Risk Assess.* **2020**, *34*, 691–707. [[CrossRef](#)]

24. Mousavi, S.N.; Farsadizadeh, D.; Salmasi, F.; Dalir, A.H.; Bocchiola, D. Analysis of minimal and maximal pressures, uncertainty and spectral density of fluctuating pressures beneath classical hydraulic jumps. *Water Supply* **2020**, *20*, 1909–1921. [[CrossRef](#)]
25. Mousavi, S.N.; Júnior, R.S.; Teixeira, E.D.; Bocchiola, D.; Nabipour, N.; Mosavi, A.; Shamshirband, S. Predictive modeling the free hydraulic jumps pressure through advanced statistical methods. *Mathematics* **2020**, *8*, 323. [[CrossRef](#)]
26. Mousavi, S.N.; Farsadizadeh, D.; Salmasi, F.; Hosseinzadeh Dalir, A. Evaluation of pressure fluctuations coefficient along the USBR Type II stilling basin using experimental results and AI models. *ISH J. Hydraul. Eng.* **2020**. [[CrossRef](#)]
27. Belanger, J.B. *Essay on the Numerical Solution of Some Problems Related to the Constant Motion of Water Flow*; Carilian-Goeury: Paris, France, 1828. (In French)
28. Hager, W.H.; Li, D. Sill-controlled energy dissipator. *J. Hydraul. Res.* **1992**, *30*, 165–181. [[CrossRef](#)]
29. Chaudhry, M.H. *Open-Channel Flow*, 2nd ed.; Springer Science & Business Media: New York, NY, USA, 2008.
30. Chanson, H. Development of the Bélanger equation and backwater equation by Jean-Baptiste Bélanger (1828). *J. Hydraul. Eng.* **2009**, *135*, 159–163. [[CrossRef](#)]
31. Bennett, N.D.; Croke, B.F.; Guariso, G.; Guillaume, J.H.; Hamilton, S.H.; Jakeman, A.J.; Marsili-Libelli, S.; Newham, L.T.; Norton, J.P.; Perrin, C. Characterising performance of environmental models. *Environ. Model. Softw.* **2013**, *40*, 1–20. [[CrossRef](#)]
32. Willmott, C.J.; Matsuura, K. Advantages of the mean absolute error (MAE) over the root mean square error (RMSE) in assessing average model performance. *Clim. Res.* **2005**, *30*, 79–82. [[CrossRef](#)]
33. Chai, T.; Draxler, R.R. Root mean square error (RMSE) or mean absolute error (MAE)?—Arguments against avoiding RMSE in the literature. *Geosci. Model Dev.* **2014**, *7*, 1247–1250. [[CrossRef](#)]
34. Willmott, C.J.; Robeson, S.M.; Matsuura, K. A refined index of model performance. *Int. J. Climatol.* **2012**, *32*, 2088–2094. [[CrossRef](#)]
35. Fiorotto, V.; Rinaldo, A. Turbulent pressure fluctuations under hydraulic jumps. *J. Hydraul. Res.* **1992**, *30*, 499–520. [[CrossRef](#)]
36. Sharma, C.; Ojha, C. Statistical parameters of hydrometeorological variables: Standard deviation, SNR, skewness and kurtosis. In *Advances in Water Resources Engineering and Management*; Springer: Singapore, 2020; Volume 39, pp. 59–70.
37. Novakoski, C.K.; Conterato, E.; Marques, M.; Teixeira, E.D.; Lima, G.A.; Mees, A. Macro-turbulent characteristics of pressures in hydraulic jump formed downstream of a stepped spillway. *Braz. J. Water Resour. (Rbrh)* **2017**, *22*. [[CrossRef](#)]
38. Prá, M.D.; Priebe, P.d.S.; Teixeira, E.D.; Marques, M.G. Evaluation of pressure fluctuation in hydraulic jump by dissociation of hydraulic forces. *Braz. J. Water Resour. (Rbrh)* **2016**, *21*, 221–231. (In Portuguese)
39. Yan, Z.-M.; Zhou, C.-T.; Lu, S.-Q. Pressure fluctuations beneath spatial hydraulic jumps. *J. Hydrodyn.* **2006**, *18*, 723–726. [[CrossRef](#)]
40. Pei-Qing, L.; Ai-Hua, L. Model discussion of pressure fluctuations propagation within lining slab joints in stilling basins. *J. Hydraul. Eng.* **2007**, *133*, 618–624. [[CrossRef](#)]
41. Wiest, R.A. *Evaluation of the Pressure Field in Hydraulic Jump Formed Downstream of a Spillway with Different Submergence Degrees*; Universidade Federal do Rio Grande do Sul: Porto Alegre, Brazil, 2008. (In Portuguese)

Publisher's Note: MDPI stays neutral with regard to jurisdictional claims in published maps and institutional affiliations.



© 2020 by the authors. Licensee MDPI, Basel, Switzerland. This article is an open access article distributed under the terms and conditions of the Creative Commons Attribution (CC BY) license (<http://creativecommons.org/licenses/by/4.0/>).